



Aalborg Universitet

**AALBORG UNIVERSITY**  
DENMARK

## **Unsteady Simulations of the Flow in a Channel Flow and a Ventilated Room Using the SST-SAS Model**

Davidson, Lars; Nielsen, Peter V.

*Publication date:*  
2006

*Document Version*  
Publisher's PDF, also known as Version of record

[Link to publication from Aalborg University](#)

*Citation for published version (APA):*  
Davidson, L., & Nielsen, P. V. (2006). Unsteady Simulations of the Flow in a Channel Flow and a Ventilated Room Using the SST-SAS Model. Aalborg: Department of Civil Engineering, Aalborg University. DCE Technical reports, No. 4

### **General rights**

Copyright and moral rights for the publications made accessible in the public portal are retained by the authors and/or other copyright owners and it is a condition of accessing publications that users recognise and abide by the legal requirements associated with these rights.

- ? Users may download and print one copy of any publication from the public portal for the purpose of private study or research.
- ? You may not further distribute the material or use it for any profit-making activity or commercial gain
- ? You may freely distribute the URL identifying the publication in the public portal ?

### **Take down policy**

If you believe that this document breaches copyright please contact us at [vbn@aub.aau.dk](mailto:vbn@aub.aau.dk) providing details, and we will remove access to the work immediately and investigate your claim.

# Unsteady Simulations of the Flow in a Channel Flow and a Ventilated Room Using the SST-SAS Model

Lars Davidson  
Peter V. Nielsen



Aalborg University  
Department of Civil Engineering

**DCE Technical Report No. 4**

Unsteady Simulations of the Flow in a Channel Flow and a  
Ventilated Room Using the SST-SAS Model

by

Lars Davidson  
Peter V. Nielsen

© Aalborg University

## Scientific Publications at the Department of Civil Engineering

**Technical Reports** are published for timely dissemination of research results and scientific work carried out at the Department of Civil Engineering (DCE) at Aalborg University. This medium allows publication of more detailed explanations and results than typically allowed in scientific journals.

**Technical Memoranda** are produced to enable the preliminary dissemination of scientific work by the personnel of the DCE where such release is deemed to be appropriate. Documents of this kind may be incomplete or temporary versions of papers—or part of continuing work. This should be kept in mind when references are given to publications of this kind.

**Contract Reports** are produced to report scientific work carried out under contract. Publications of this kind contain confidential matter and are reserved for the sponsors and the DCE. Therefore, Contract Reports are generally not available for public circulation.

**Lecture Notes** contain material produced by the lecturers at the DCE for educational purposes. This may be scientific notes, lecture books, example problems or manuals for laboratory work, or computer programs developed at the DCE.

**Theses** are monographs or collections of papers published to report the scientific work carried out at the DCE to obtain a degree as either PhD or Doctor of Technology. The thesis is publicly available after the defence of the degree.

**Latest News** is published to enable rapid communication of information about scientific work carried out at the DCE. This includes the status of research projects, developments in the laboratories, information about collaborative work and recent research results.

Published 2006 by  
Aalborg University  
Department of Civil Engineering  
Sohngaardsholmsvej 57,  
DK-9000 Aalborg, Denmark

Printed in Aalborg at Aalborg University

ISSN 1901-726X  
DCE Technical Report No. 4

# Unsteady simulations of the flow in a channel flow and a ventilated room using the SST-SAS model\*

Lars Davidson<sup>†</sup> and Peter V. Nielsen<sup>‡</sup>

<sup>†</sup>Division of Fluid Dynamics, Department of Applied Mechanics  
Chalmers University of Technology, SE-412 96 Göteborg, Sweden

<sup>‡</sup>Building Technology and Structural Engineering  
Aalborg University, DK-9000 Aalborg, Denmark

## 1 Abstract

The SAS model (Scale Adapted Simulation) was invented by Menter and his co-workers. The idea behind the SST-SAS model is to add an additional production term – the SAS term – in the  $\omega$  equation which is sensitive to resolved (i.e. unsteady) fluctuations. In regions where the flow is on the limit of going unsteady, the object of the SAS term is to increase  $\omega$ . The result is that  $k$  and  $\nu_t$  are reduced so that the dissipating (damping) effect of the turbulent viscosity on the resolved fluctuations is reduced, thereby promoting the momentum equations to switch from steady to unsteady mode.

The SST-SAS model is evaluated for two flows: developing channel flow and the flow in a three-dimensional ventilated room. Unsteady inlet boundary conditions are prescribed in both cases by superimposing isotropic synthetic fluctuations on a steady inlet boundary velocity profile.

## 2 The $k - kL$ Turbulence Model

### 2.1 Derivation

Rotta (1972) derived an exact equation for  $kL$  based on the integral length scale.

$$kL = \frac{3}{16} \int R_{ii}(\mathbf{x}, \eta) d\eta, \quad R_{ij} = \overline{u_i(\mathbf{x})u_j(\mathbf{x} + \eta)} \quad (1)$$

In all two-equation models there is one production term and one destruction term. Rotta's  $kL$  equation includes two production terms, namely (here

---

\*The initial part of this work was carried out during the first author's stay at Aalborg University

given in boundary-layer form)

$$S_{kL} = - \underbrace{\frac{3}{16} \frac{\partial \bar{u}(\mathbf{x})}{\partial y} \int R_{21} d\eta}_I - \underbrace{\frac{3}{16} \int \frac{\partial \bar{u}(\mathbf{x} + \eta)}{\partial y} R_{12} d\eta}_{II} \quad (2)$$

To simplify the second term, Rotta used Taylor expansion so that

$$\frac{\partial \bar{u}(\mathbf{x} + \eta)}{\partial y} = \underbrace{\frac{\partial \bar{u}(\mathbf{x})}{\partial y}}_a + \underbrace{\eta \frac{\partial^2 \bar{u}(\mathbf{x})}{\partial y^2}}_b + \underbrace{\frac{1}{2} \eta^2 \frac{\partial^3 \bar{u}(\mathbf{x})}{\partial y^3}}_c + \dots \quad (3)$$

The first term,  $a$ , is incorporated in  $S_{kL,I}$ . Rotta set the second term,  $b$ , to zero

$$\frac{\partial^2 \bar{u}(\mathbf{x})}{\partial y^2} \int_{-\infty}^{+\infty} R_{12} \eta d\eta = 0 \quad (4)$$

because in homogeneous shear flow  $R_{12}(\eta)$  is antisymmetric with respect to  $\eta$ . The second term in Eq. 2 was consequently modelled with the third term,  $c$ , including the third velocity gradient  $\partial^3 \bar{u} / \partial y^3$ .

Menter and Egorov (2004) argue that homogeneous flow is not a relevant flow case, because then the second velocity gradient is zero anyway. They propose to model the  $S_{kL,II}$ -term using the second velocity gradient as (Menter and Egorov, 2004, 2005):

$$S_{kL,IIb} = - \frac{3}{16} \int \frac{\partial \bar{u}(\mathbf{x} + \eta)}{\partial y} R_{12} d\eta = - |\overline{uv}| \left| \frac{\partial^2 \bar{u}(\mathbf{x})}{\partial y^2} \right| L^2 \quad (5)$$

The eddy-viscosity assumption for the shear stress gives  $|uv| = \nu_t |\partial \bar{u} / \partial y|$ . In three-dimensional flow the shear stress can be estimated by an eddy-viscosity expression  $\nu_t (2 \bar{s}_{ij} \bar{s}_{ij})^{0.5}$ . Using a general formula for the second derivative of the velocity we get

$$\begin{aligned} S_{kL,IIb} &= -\nu_t S |U''| L^2 \\ S &= (2 \bar{s}_{ij} \bar{s}_{ij})^{0.5} \\ U'' &= \left( \frac{\partial^2 \bar{u}_i}{\partial x_j \partial x_j} \frac{\partial^2 \bar{u}_i}{\partial x_j \partial x_j} \right)^{0.5} \end{aligned} \quad (6)$$

In the  $k - kL$  model the turbulent viscosity,  $\nu_t$ , and the dissipation term,  $\varepsilon$ , in the  $k$  equation have the form

$$\nu_t = c_1 \frac{kL}{k^{1/2}} \quad (7)$$

$$\varepsilon = \frac{k^{5/2}}{kL} \quad (8)$$

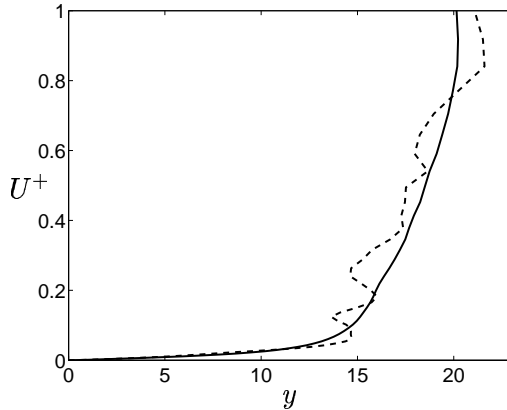


Figure 1: Velocity profiles from a DNS of channel flow. Solid line: time-averaged velocity; dashed line: instantaneous velocity.

The term  $S_{kl,IIb}$  in the  $kL$  equation is a sink term that reduces  $kL$ . The result is that the turbulent viscosity is reduced because  $kL$  appears in the nominator of the expression for  $\nu_t$ , see Eq. 7. This reduction is somewhat diminished since a decrease in  $kL$  also reduces  $k$  via an increase of the dissipation term,  $\varepsilon$ , see Eq. 8. However, since  $kL$  appears directly in  $\nu_t$  it is expected that the overall effect of a large  $S_{kL,IIb}$  will be a decrease in  $\nu_t$ .

The source term  $S_{kL,IIb}$  includes the second velocity gradient. The von Kármán length scale

$$L_{vK,1D} = \kappa \left| \frac{\partial \langle \bar{u} \rangle / \partial y}{\partial^2 \langle \bar{u} \rangle / \partial y^2} \right| \quad (9)$$

also includes the second velocity gradient. This is interesting because, as noted by Menter and Egorov (2004), the von Kármán decreases when the momentum equations resolve (part of) the turbulence. The von Kármán length scale is smaller for an instantaneous velocity profile than for a time averaged velocity, see Fig. 1. When doing URANS or DES, the momentum equations are triggered through instabilities to go unsteady in regions where the grid is fine enough. In URANS or in DES operating in RANS mode, high turbulent viscosity dampens out these instabilities. In many cases this is an undesired feature, because if the flow wants to go unsteady, it is usually a bad idea to force the equations to stay steady. One reason is that there may not be any steady solution. Hence, the equations will not converge. Another reason is that if the numerical solution wants to go unsteady, the large turbulent scales will be resolved instead of being modelled. This leads to a more accurate prediction of the flow.

The role of the term  $S_{kL,IIb}$  is that this term gets large when unsteady resolved velocities appear somewhere in the flow. As discussed above, this will lead to a reduced turbulent viscosity which means that the resolved fluctuations are less likely to be dampened. This feature led Menter and his



co-workers (Menter et al., 2003; Menter and Egorov, 2004, 2005) to introduce the von Kármán length scale in a one-equation model, in a  $k - k^{1/2}L$  model and in a  $k - \omega$  SST model. In the present study, we will use and evaluate the modified  $k - \omega$  SST model.

## 2.2 The Second derivative

To compute  $U''$  in Eq. 6, we need to compute the second velocity gradients. In finite volume methods there are two main options for computing second derivatives.

Option I: compute the first derivatives at the faces

$$\left(\frac{\partial u}{\partial y}\right)_{j+1/2} = \frac{u_{j+1} - u_j}{\Delta y}, \quad \left(\frac{\partial u}{\partial y}\right)_{j-1/2} = \frac{u_j - u_{j-1}}{\Delta y}$$

and then

$$\Rightarrow \left(\frac{\partial^2 u}{\partial y^2}\right)_j = \frac{u_{j+1} - 2u_j + u_{j-1}}{(\Delta y)^2} + \frac{(\Delta y)^2}{12} \frac{\partial^4 u}{\partial y^4}$$

Option II: compute the first derivatives at the center

$$\left(\frac{\partial u}{\partial y}\right)_{j+1} = \frac{u_{j+2} - u_j}{2\Delta y}, \quad \left(\frac{\partial u}{\partial y}\right)_{j-1} = \frac{u_j - u_{j-2}}{2\Delta y}$$

and then

$$\Rightarrow \left(\frac{\partial^2 u}{\partial y^2}\right)_j = \frac{u_{j+2} - 2u_j + u_{j-2}}{4(\Delta y)^2} + \frac{(\Delta y)^2}{3} \frac{\partial^4 u}{\partial y^4}$$

In the present work Option I is used unless otherwise stated.

## 2.3 The $k - \omega$ SST model

The standard  $k - \omega$  SST model reads (Menter, 1994)

$$\begin{aligned} \frac{\partial k}{\partial t} + \frac{\partial}{\partial x_j}(\bar{u}_j k) &= \frac{\partial}{\partial x_j} \left[ \left( \nu + \frac{\nu_t}{\sigma_k} \right) \frac{\partial k}{\partial x_j} \right] + P_k - \beta^* k \omega \\ \frac{\partial \omega}{\partial t} + \frac{\partial}{\partial x_j}(\bar{u}_j \omega) &= \frac{\partial}{\partial x_j} \left[ \left( \nu + \frac{\nu_t}{\sigma_\omega} \right) \frac{\partial \omega}{\partial x_j} \right] + P_\omega - \beta \omega^2 \\ &\quad + 2(1 - F_1) \sigma_{\omega 2} \frac{1}{\omega} \frac{\partial k}{\partial x_i} \frac{\partial \omega}{\partial x_i} \\ F_1 &= \tanh(\xi^4), \quad \xi = \min \left[ \max \left\{ \frac{\sqrt{k}}{\beta^* \omega y}, \frac{4\sigma_{\omega 2} k}{CD_\omega y^2} \right\} \right] \\ \nu_t &= \frac{a_1 k}{\max(a_1 \omega, SF_2)}, \quad P_\omega = \alpha \frac{P_k}{\nu_t} \\ F_2 &= \tanh(\eta^2), \quad \eta = \max \left\{ \frac{2k^{1/2}}{\beta^* \omega y}, \frac{500\nu}{y^2 \omega} \right\} \end{aligned} \quad (10)$$

Now we wish to transform the  $S_{kL,IIb}$  term in the  $k - kL$  model to the  $k - \omega$  model. The  $kL$  equation (expressed in the dependent variables  $k$  and  $kL$ ) can be transformed term by term to the  $\omega$  equation (expressed in the dependent variables  $k$  and  $\omega = k^{3/2}/(kL)$ ). The transformation reads

$$\frac{d\omega}{dt} = \frac{3}{2} \frac{k^{1/2}}{(kL)} \frac{dk}{dt} - \frac{k^{3/2}}{(kL)^2} \frac{d(kL)}{dt} \quad (11)$$

The last term is used to transform the  $S_{kL,IIb}$  term (see Eq. 6) which gives

$$S_{\omega,IIb} = -\frac{k^{3/2}}{(kL)^2} (-\nu_t S |U''| L^2) = \frac{1}{k^{1/2} L} \nu_t S |U''| L \propto S |U''| L \quad (12)$$

The second velocity gradient,  $\partial^2 \bar{u} / \partial y^2$ , appears in the definition of the von Kármán length scale, and it is given in Eq. 9 in boundary layer form.  $S$  and  $U''$  in Eq. 12 correspond to one form of first and second velocity gradients in three-dimensional flow. Using  $S$  and  $U''$  in Eq. 9 and inserting it in Eq. 12 gives

$$S_{\omega,IIb} = \tilde{\zeta}_2 \kappa S^2 \frac{|U''|}{\kappa S} L = \tilde{\zeta}_2 \kappa S^2 \frac{L}{L_{vK,3D}} \quad (13)$$

$$L_{vK,3D} = \kappa \frac{S}{|U''|}$$

When transforming the  $k - kL$  equation a term involving derivatives of  $\omega$  appears. To preserve the SST model in the URANS region, a term with derivatives of  $\partial k / \partial x_i$  is also included. The final form of the additional term in the  $\omega$  equation reads (Menter and Egorov, 2005)

$$S_\omega = F_{SAS} \max(T_1 - T_2, 0)$$

$$T_1 = \tilde{\zeta}_2 \kappa S^2 \frac{L}{L_{vK,3D}}$$

$$T_2 = \frac{2k}{\sigma_\Phi} \max\left(\frac{1}{\omega^2} \frac{\partial \omega}{\partial x_j} \frac{\partial \omega}{\partial x_j}, \frac{1}{k^2} \frac{\partial k}{\partial x_j} \frac{\partial k}{\partial x_j}\right) \quad (14)$$

$$L = \frac{k^{1/2}}{\omega c_\mu^{1/4}}$$

## 2.4 Evaluation of the von Kármán length scale in fully developed channel flow

In Fig. 2 the turbulent length scale,  $\langle L_{vK,3D} \rangle$ , is evaluated using DNS data of fully developed channel flow. When using DNS data only viscous dissipation of resolved turbulence affects the equations. This implies that the smallest scales that can be resolved are related to the grid scale. The von Kármán

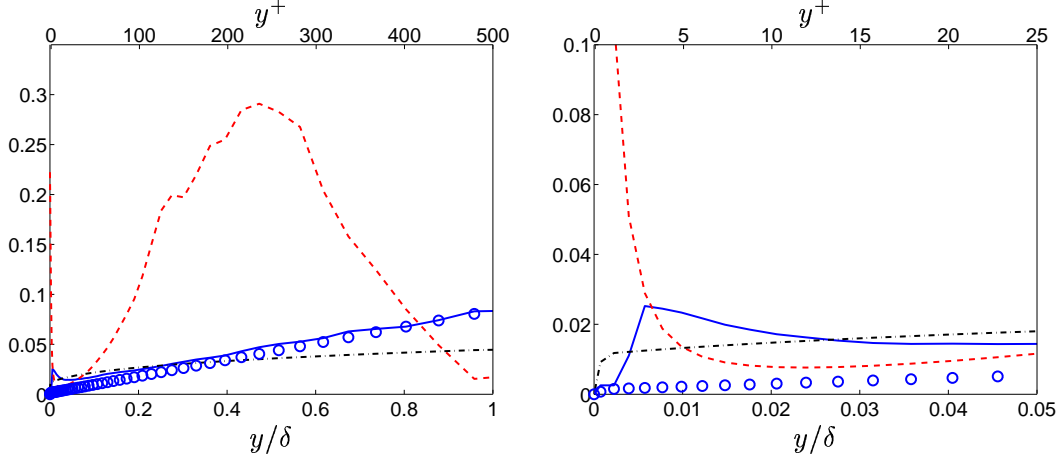


Figure 2: Turbulent length scales in fully developed channel flow. Left: global view; right: zoom. DNS.  $96^3$  mesh.  $Re_\tau = 500$ .  $\Delta x/\delta = 0.065$ ,  $\Delta z/\delta = 0.016$ ,  $y$ -stretching of 9%. — :  $\langle L_{vK,3D} \rangle$ ; - - - :  $L_{vK,1D}$ ; ··· :  $(\Delta x \Delta y \Delta z)^{1/3}$ ; ○ :  $\Delta y$ .

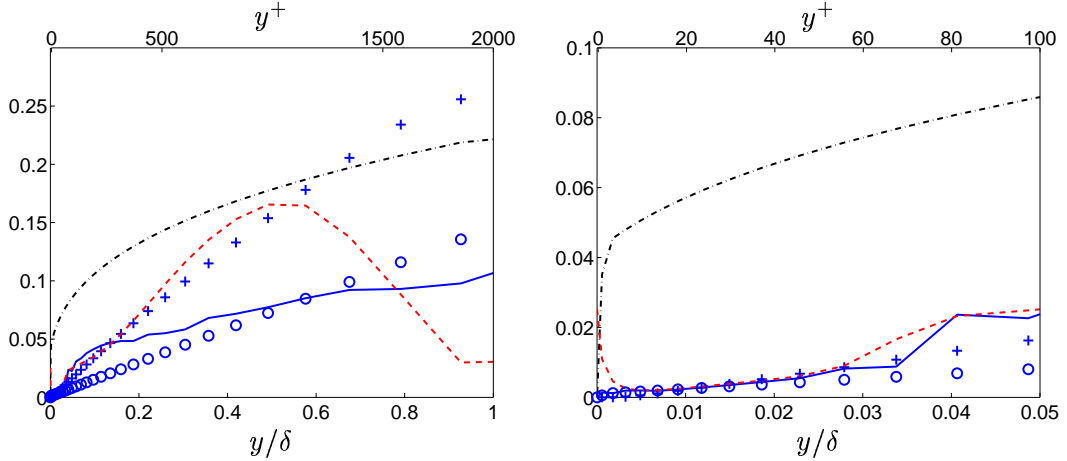


Figure 3: Turbulent length scales in fully developed channel flow. Hybrid LES-RANS. Left: global view; right: zoom.  $32 \times 64 \times 32$  mesh.  $Re_\tau = 2000$ .  $\Delta x/\delta = 0.39$ ,  $\Delta z/\delta = 0.19$ ,  $y$ -stretching of 17%. — :  $\langle L_{vK,3D} \rangle$ ; - - - :  $L_{vK,1D}$ ; ··· :  $(\Delta x \Delta y \Delta z)^{1/3}$ ; ○ :  $\Delta y$ ; + :  $\ell_{k-\omega} = k^{0.5}/(c_\mu^{1/4} \omega)$ .

length scale based on instantaneous velocities,  $\langle L_{vK,3D} \rangle$ , is presented in the Fig. 2. For  $y > 0.2$ , its magnitude is close to  $\Delta y$  which confirms that the von Kármán length scale is related to the smallest resolvable scales. Closer to the wall,  $\langle L_{vK,3D} \rangle$  increases slightly whereas  $\Delta y$  continues to decrease.

The von Kármán length scale,  $L_{vK,1D}$ , based on the averaged velocity profile  $\langle \bar{u} \rangle = \langle \bar{u} \rangle(y)$  is also included in Fig. 2, and as can be seen it is much larger than  $\langle L_{vK,3D} \rangle$ . Near the wall  $L_{vK,1D}$  increases because the time-average second derivative,  $\partial^2 \langle \bar{u} \rangle / \partial y^2$ , goes to zero as the wall is approached.

No such behavior is seen for the three-dimensional formulation,  $\langle L_{vK,3D} \rangle$ .

In Fig. 3, data from hybrid LES-RANS are used (taken from Davidson and Billson (2006)). When using hybrid LES-RANS, part of the turbulence is resolved and part of the turbulence is modelled. The resolved turbulence is dissipated by a modelled dissipation,  $-2\langle \nu_T \bar{s}_{ij} \bar{s}_{ij} \rangle$  ( $\nu_T$  denotes SGS or RANS turbulent viscosity), and  $\nu_T \gg \nu$ . As a result, the length scale of the smallest resolved turbulence is larger in hybrid LES-RANS than in DNS. Close to the wall in the URANS region ( $y < 0.031\delta$ ), the resolved turbulence is dampened by the high turbulent viscosity, and as a result  $\langle L_{vK,3D} \rangle$  follows closely  $L_{vK,1D}$ .

The RANS turbulent length scale,  $\ell_{k-\omega}$ , from a 1D RANS simulation at  $Re_\tau = 2000$  with the SST model is also included in Fig. 3. In the inner region ( $y < 0.5\delta$ ), its behavior is close to that of the von Kármán length scale,  $L_{vK,1D}$ . In the center region the RANS turbulent length scale continues to increase whereas the von Kármán length scale,  $L_{vK,1D}$ , goes to zero.

Two filter scales are included in Figs. 2 and 3. In the DNS-simulations,  $\Delta y < (\Delta x \Delta y \Delta z)^{1/3}$  near the wall, whereas far from the wall  $\Delta y > (\Delta x \Delta y \Delta z)^{1/3}$  because of the stretching in the  $y$  direction and because of small  $\Delta x$  and  $\Delta z$ . In the hybrid simulations, it can be noted that the three-dimensional filter width is approximately twice as large as the three-dimensional formulation of the von Kármán length scale, i.e.  $(\Delta x \Delta y \Delta z)^{1/3} > \langle L_{vK,3D} \rangle$ .

### 3 The Numerical Method

An incompressible, finite volume code with a non-staggered grid arrangement is used (Davidson and Peng, 2003). For space discretization, central differencing is used for all terms. The Crank-Nicholson scheme is used for time discretization of all equations. The numerical procedure is based on an implicit, fractional step technique with a multigrid pressure Poisson solver (Emvin, 1997).

### 4 Inlet Conditions

Inlet fluctuating velocity fields ( $u', v', w'$ ) are at each time step created at the inlet  $y - z$  plane using synthetic isotropic fluctuations (Billson, 2004). However, they are independent of each other, and thus their time correlation will be zero. This is unphysical. To create correlation in time, new fluctuating velocity fields  $\mathcal{U}', \mathcal{V}', \mathcal{W}'$  are computed as (Billson, 2004; Billson

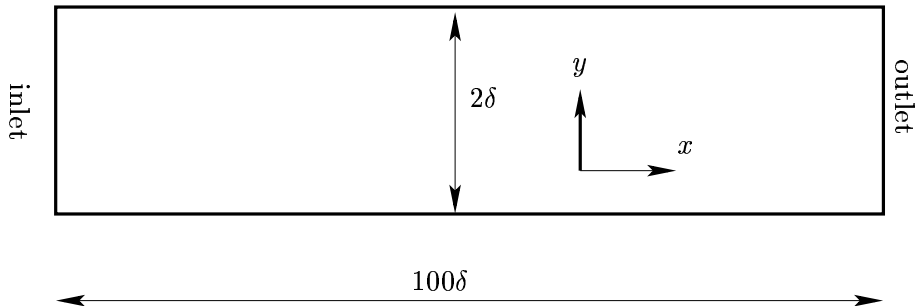


Figure 4: Channel with inlet and outlet.

et al., 2003)

$$\begin{aligned}
 (\mathcal{U}')^m &= a(\mathcal{U}')^{m-1} + b(u')^m \\
 (\mathcal{V}')^m &= a(\mathcal{V}')^{m-1} + b(v')^m \\
 (\mathcal{W}')^m &= a(\mathcal{W}')^{m-1} + b(w')^m
 \end{aligned}
 \tag{15}$$

where  $m$  denotes time step number,  $a = \exp(-\Delta t/\mathcal{T})$  and  $b = (1 - a^2)^{0.5}$ . The time correlation of  $\mathcal{U}'_i$  will be equal to  $\exp(-\Delta t/\mathcal{T})$ , where  $\mathcal{T}$  is proportional to the turbulent time scale. The inlet boundary conditions are prescribed as

$$\begin{aligned}
 \bar{u}(0, y, z, t) &= U_{in}(y) + u'_{in}(y, z, t) \\
 \bar{v}(0, y, z, t) &= v'_{in}(y, z, t) \\
 \bar{w}(0, y, z, t) &= w'_{in}(y, z, t)
 \end{aligned}
 \tag{16}$$

The mean inlet velocity,  $U_{in}(y)$  is taken from fully developed channel flow predicted with the SST-URANS model.

## 5 Results

### 5.1 Channel Flow

A  $256 \times 64 \times 32$  node mesh ( $x$ , streamwise;  $y$ , wall-normal;  $z$ , spanwise) has been used. The size of the computational domain is  $x_{max} = 100$ ,  $y_{max} = 2$  (geometric stretching of 17%) and  $z_{max} = 6.28$ , see Fig. 4. This gives a  $\Delta x^+$  and  $\Delta z^+$  of approximately 785 and 393, respectively and  $y^+ < 1$  near the walls, expressed in inner scaling. In outer scaling  $\delta/\Delta x \simeq 2.5$  and  $\delta/\Delta z \simeq 5$ . The time step was set to  $\Delta t u_\tau/\delta = 4.91 \cdot 10^{-3}$ . The Reynolds number is  $Re_\tau = u_\tau \delta/\nu = 2000$ . Neumann boundary conditions are prescribed at the outlet.

Below the results using the standard SST-URANS model and the SST-SAS model are presented. In Fig 5 the velocity profiles are shown and the

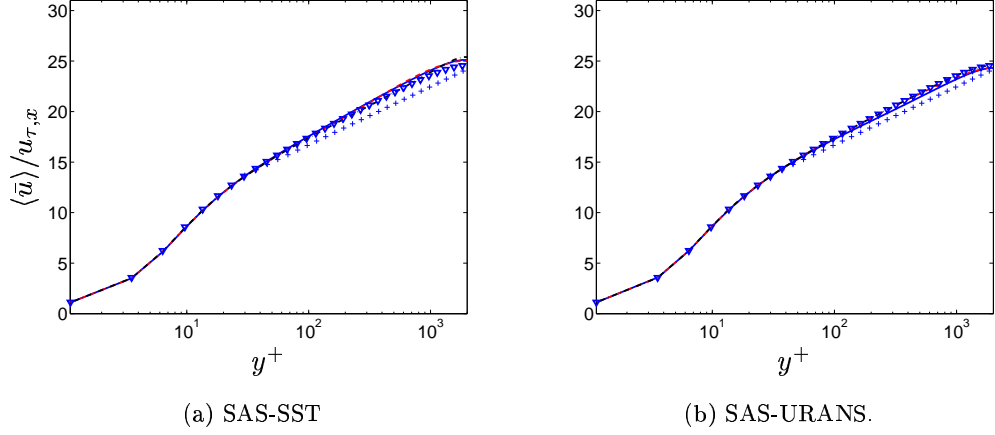


Figure 5: Velocity profiles. — :  $x/\delta = 3.33$ ; - - - :  $x/\delta = 23$ ; ··· :  $x/\delta = 97$ ; +:  $2.5 \ln(y^+) + 5.2$ ;  $\nabla$ : from a 1D simulation with the SST model.

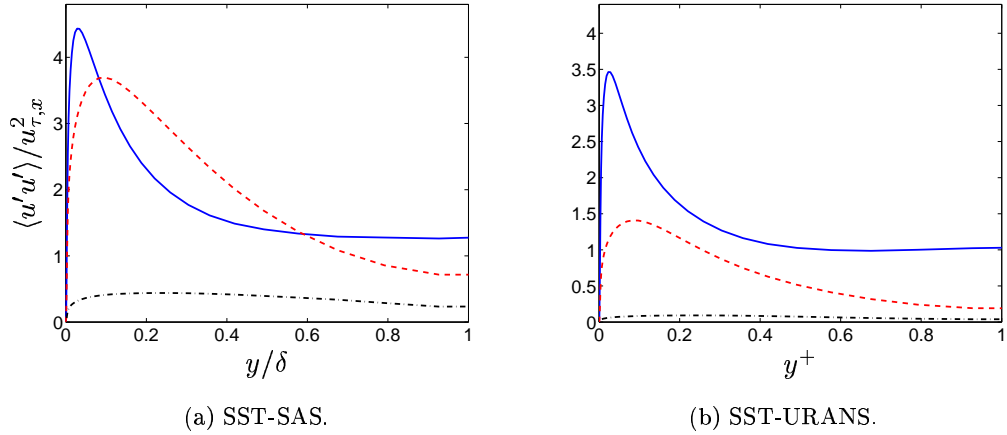


Figure 6: Streamwise resolved normal stresses. — :  $x/\delta = 3.33$ ; - - - :  $x/\delta = 23$ ; ··· :  $x/\delta = 97$ .

results obtained with the two models are very similar. Figures 6 and 7 show the predicted resolved Reynolds stresses. As can be seen, the stresses predicted with the SAS model decay at a slower rate than those predicted with the SST-URANS model. The reason is that the turbulent viscosity is smaller with the SST-SAS model than with the SST-URANS model, which makes the dissipation of the resolved fluctuations smaller with the former model. It can be noted that at the end of the channel ( $x/\delta = 97$ ), the turbulent viscosity with the SST-URANS model is equal to the turbulent viscosity

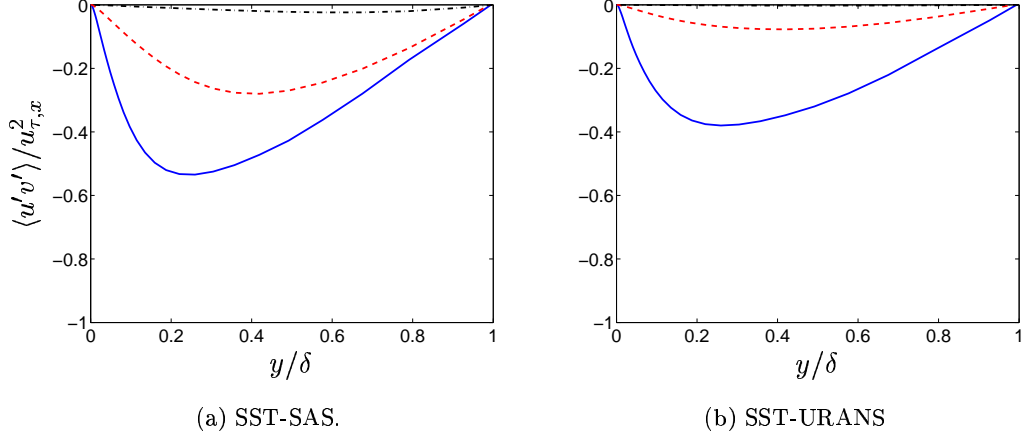


Figure 7: Resolved shear stresses. — :  $x/\delta = 3.33$ ; - - - :  $x/\delta = 23$ ; . . . :  $x/\delta = 97$ .

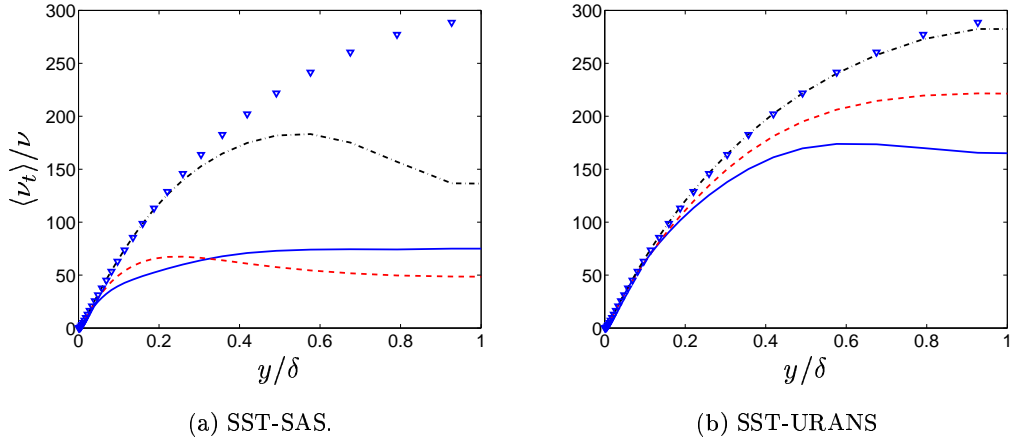


Figure 8: Turbulent viscosity. — :  $x/\delta = 3.33$ ; - - - :  $x/\delta = 23$ ; . . . :  $x/\delta = 97$ ;  $\nabla$ : from a 1D simulation with the SST model.

predicted in a 1D channel using the SST-URANS model (see Fig. 8b) and that the resolved stresses are zero. Hence the flow has returned to fully steady conditions.

Figure 9a presents the ratio of the turbulent and von Kármán length scales. As expected, the von Kármán is largest near the inlet where the resolved fluctuations are largest. Near the inlet the von Kármán length scale is more than twice as large as the turbulent length scale,  $L$ . When the resolved stresses far downstream become very small (i.e the flow goes

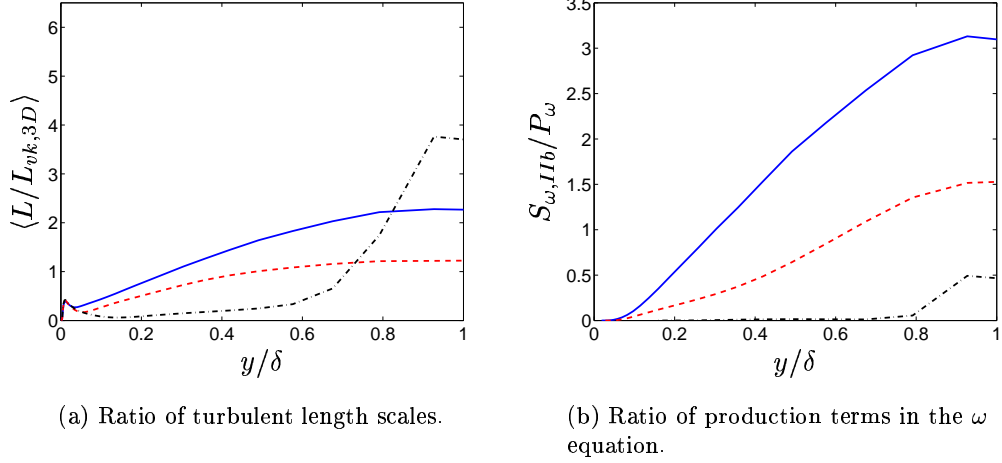


Figure 9: SAS-SST model. SAS terms. — :  $x/\delta = 3.33$ ; - - - :  $x/\delta = 23$ ; - · - :  $x/\delta = 97$ .

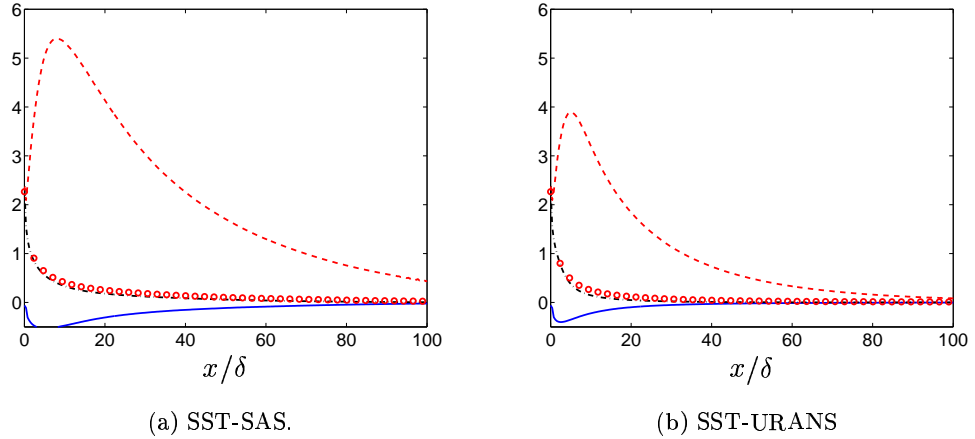


Figure 10: Decay of resolved stresses. — :  $\langle u'v' \rangle / u_{\tau,x}^2$ ; - - - :  $\langle u'u' \rangle / u_{\tau,x}^2$ ; - · - :  $\langle v'v' \rangle / u_{\tau,x}^2$ ; ○ :  $\langle w'w' \rangle / u_{\tau,x}^2$ .

towards a steady solution), the ratio near the centerline increases since the von Kármán length scale for steady flow is small in this region, cf. Fig. 3a.

The ratio of the production term,  $P_{\omega}$ , and the SAS term,  $S_{\omega}$ , in the  $\omega$  equation is presented in Fig. 9b. Near the inlet the SAS term is large, more than three times  $P_{\omega}$ , and further downstream it decreases as the resolved fluctuations are dampened.

Figure 10 presents the maximum of the resolved stresses vs.  $x$ . Here it is



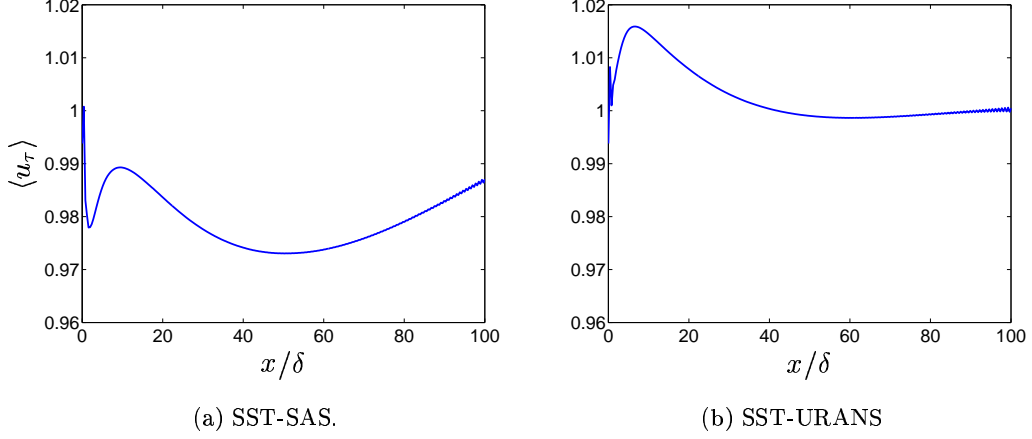


Figure 11: Friction velocities.

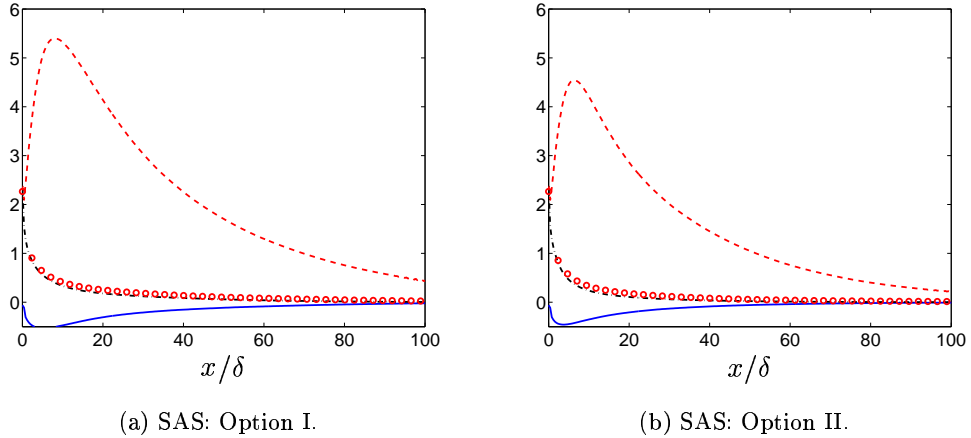


Figure 12: SAS model. Decay of resolved stresses. Two different options for computing the second velocity derivatives, see Section 2.2. — :  $\langle u'v' \rangle / u_{\tau,x}^2$ ; - - - :  $\langle u'u' \rangle / u_{\tau,x}^2$ ; ··· :  $\langle v'v' \rangle / u_{\tau,x}^2$ ; ○ :  $\langle w'w' \rangle / u_{\tau,x}^2$ .

again illustrated that the resolved stresses are dampened much faster with the SST-URANS model than with the SST-SAS model.

The friction velocities are presented in Fig. 11. In the developing unsteady region the friction velocity differs from its steady-state value of 1, and as the resolved fluctuations are dampened further downstream the friction velocity approaches towards one.

Figure 12 presents the maximum of the resolved stresses vs.  $x$ . Option I and II for computing the second velocity derivatives in  $U''$  (see Section 2.2)

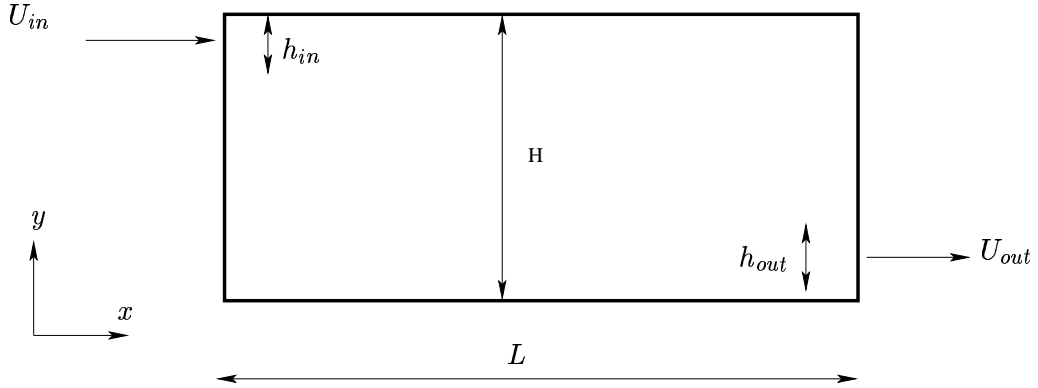


Figure 13: Configuration of ventilated room.  $L = 3H$ ,  $h_{in}/H = 0.056$ ,  $h_{out}/H = 0.16$ . Width of room, inlet and outlet is  $Z_{max} = H$ .

are compared. Option II uses only every second node, and hence  $U''$  becomes smaller ( $S_\omega$  larger) than with Option I. Hence the turbulent viscosity is smaller with Option I compared with Option II and this is what makes the resolved stresses larger with Option I than with Option II, see Figure 12.

## 5.2 Ventilated Room

The flow in a ventilated room has been computed, see Fig. 13. Time averaged inlet profiles of  $U$ ,  $k$  and  $\omega$  are taken from 1D RANS simulation of channel flow. Synthetic fluctuations are superimposed as described in Section 4. Wall functions based on the log-law are used if  $y^+ > 11$ ; otherwise the linear law is used. The former boundary condition is implemented by prescribing a turbulent viscosity at the wall (Davidson and Farhanieh, 1995). The distance from the wall-adjacent nodes to the wall vary between 5 and 30 (wall units). Equi-distant mesh has been used in the spanwise direction. The flow in the room is simulated using the SST-SAS and the SST-URANS model. The SST-URANS model gives virtually identical results as the steady SST model with steady inlet boundary conditions. All results presented below have been averaged (denoted by  $\langle \cdot \rangle$ ) in time and spanwise direction over  $0.2H \leq z \leq 0.8H$ .

The velocity profiles are compared with experiments in Figs. 14 and 15. In the wall-jet region both models give good agreement with experiments (the SST-URANS slightly better). In the recirculation region, however, the SST-URANS yields a much too strong back-flow, whereas the flow predicted with the SST-SAS model agrees well with experiments.

Figures 16 and 17 present the streamwise normal stresses, both resolved and modelled. The SST-SAS model yields resolved fluctuations which are of the same magnitude as the modelled ones and that are larger than the modelled fluctuations in the stagnant region in the middle part of the room.

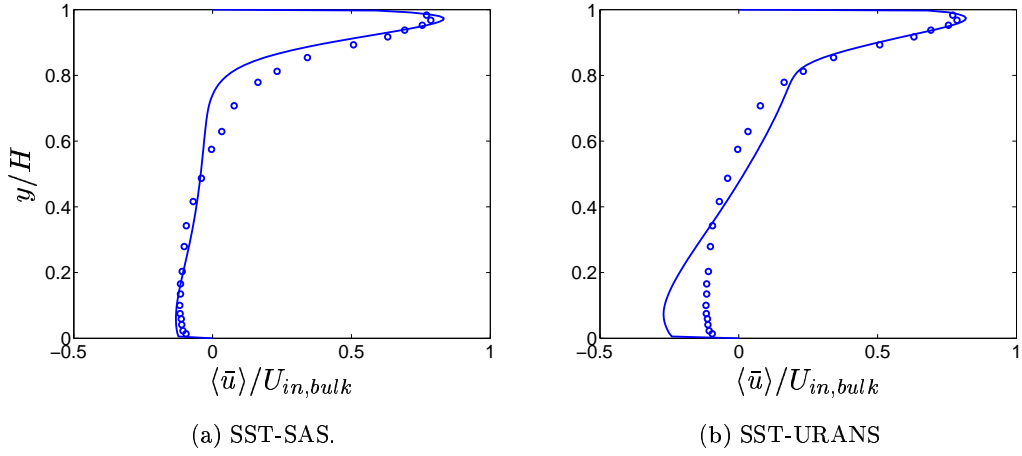


Figure 14: Velocity profiles.  $x = H$ . Markers: experiments.

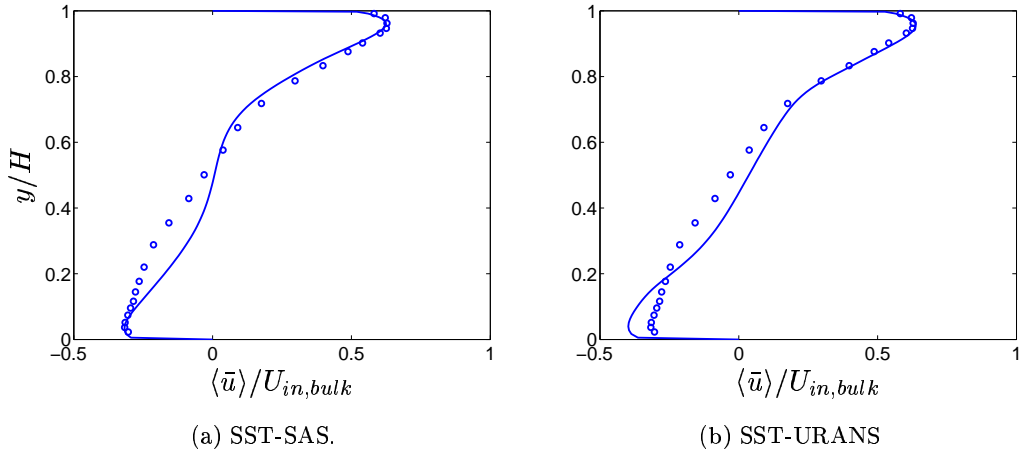


Figure 15: Velocity profiles.  $x = 2H$ . Markers: experiments.

The SST-URANS model on the other hand yields resolved fluctuations which are close to zero everywhere. Figure 18 compares the additional production term  $S_\omega$  – i.e the SAS term – in the  $\omega$  with the usual production term  $P_\omega$ .  $S_\omega$  is at its largest in the region below the wall jet where it is comparable to  $P_\omega$ . The larger the SAS term, the larger  $\omega$ , which decreases the modelled turbulent kinetic energy,  $k$ , and the turbulent viscosity,  $\nu_t$ . Figures 19 and 20 show that in the wall jet the turbulent viscosities predicted with the two models are fairly similar, but in the middle of the room – where the SAS term is large – the turbulent viscosity predicted with the SAS-SST model is much smaller than that predicted with the SST-URANS model.

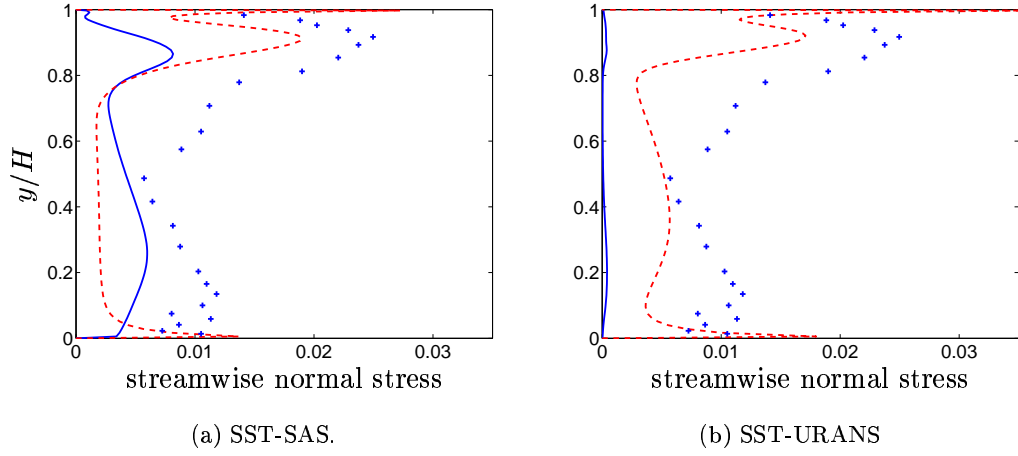


Figure 16: — : resolved turbulent stress  $\langle u'u' \rangle / U_{in,bulk}^2$ ; - - - : modelled turbulent stress  $2k / (3U_{in,bulk}^2)$ .  $x = H$ .

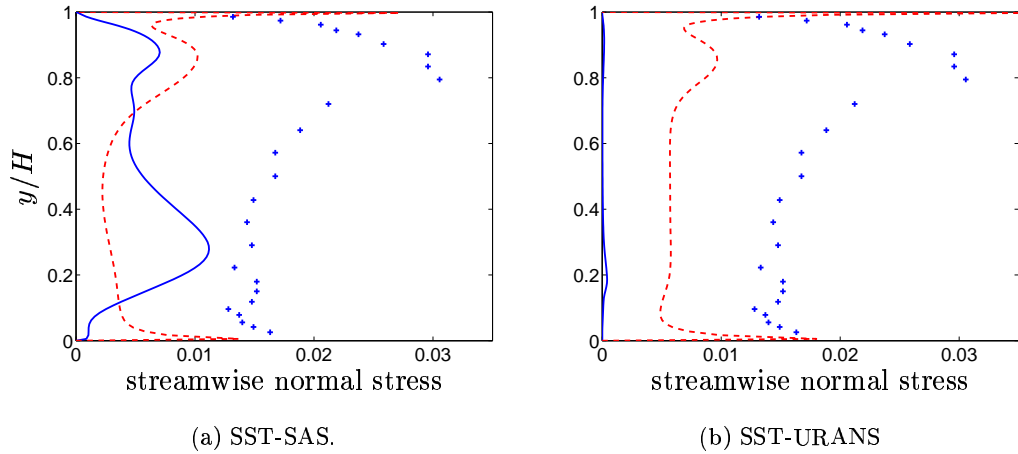


Figure 17: — : resolved turbulent stress  $\langle u'u' \rangle / U_{in,bulk}^2$ ; - - - : modelled turbulent stress  $2k / (3U_{in,bulk}^2)$ .  $x = 2H$ .

The shear stresses at  $x = H$  and  $x = 2H$  are shown in Figs. 21 and 22. In the wall region the modelled shear stresses predicted with the two models are similar, because the velocity profiles and the turbulent viscosities predicted with the two models are similar. The modelled shear stress obtained in the middle of the room with the SST-URANS model is larger than that obtained with the SST-SAS model because of the larger turbulent viscosity in the former case. The resolved shear stress predicted with the SST-URANS

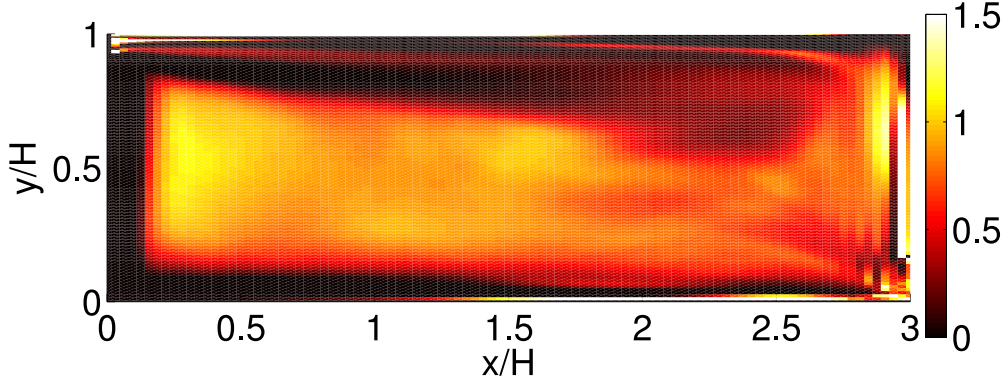


Figure 18: Ratio of the SAS term and the production in the  $\omega$  equation, i.e.  $S_\omega/P_\omega$ .

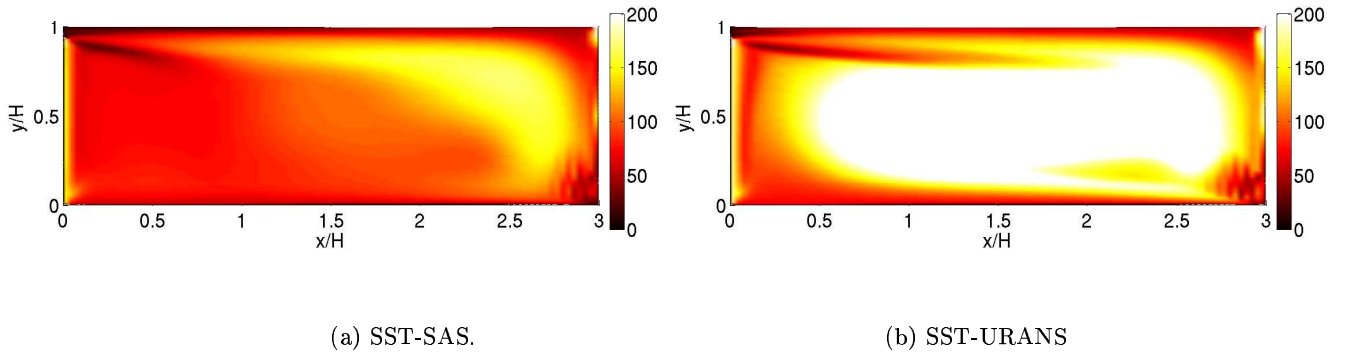


Figure 19: Turbulent viscosity  $\nu_t/\nu$ .

model is close to zero everywhere. The resolved shear stress obtained with the SST-SAS model is larger than the modelled one on the stagnant region in the middle of the room.

## 6 Conclusions

The SST-SAS model has been compared with the standard SST-URANS model in channel flow and ventilated room flow. Unsteady, turbulent inlet boundary conditions are prescribed in both cases. It has been confirmed that the SAS term acts as expected: it reduces the turbulent viscosity compared to the SST-URANS model and the resolved fluctuations are much larger with the SST-SAS model than with the SST-URANS model.

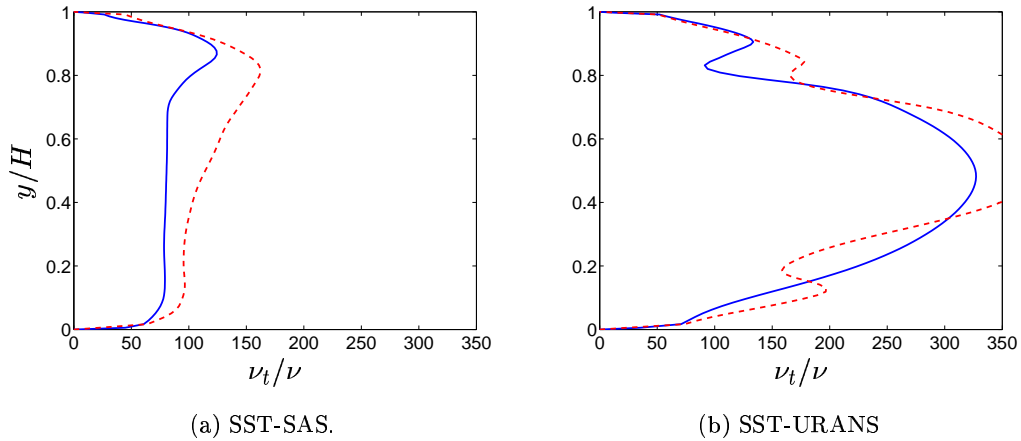


Figure 20: Turbulent viscosity profiles. — :  $x = H$ .; - - - : modelled.  $x = 2H$ .

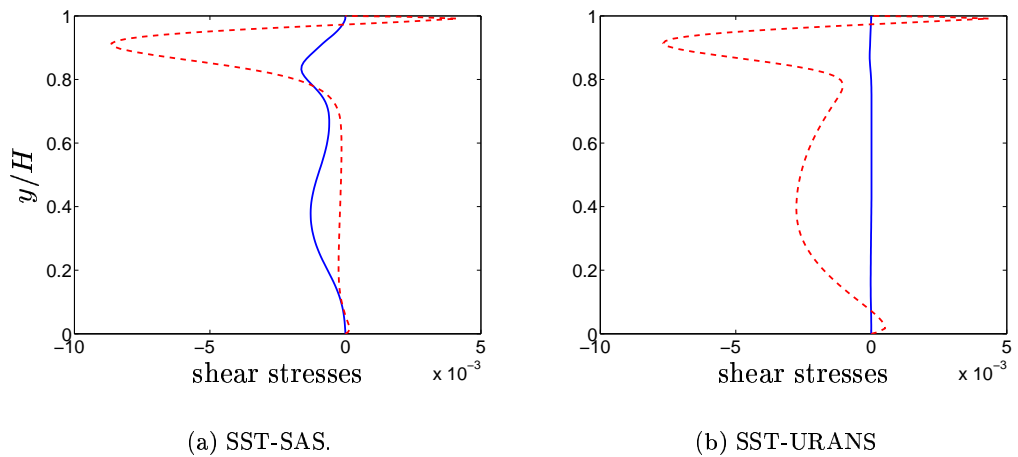


Figure 21: Shear stresses. — : resolved; - - - : modelled.  $x = H$ .

The grid used in the channel flow simulations is very coarse ( $\delta/\Delta x = 2.5$  and  $\delta/\Delta z = 5$ , where  $\delta$  denotes half-channel width). Hence, resolved turbulent fluctuations can not be sustained with any of the models. The damping of resolved turbulence by the coarse grid and the relatively large turbulent viscosities is too large. The prescribed turbulent fluctuations in the channel flow decay at a much slower rate with the SAS-SST model than with the SAS-URANS model.

The flow in the ventilated room is in better agreement with the experiments when using the SST-SAS model than when using the SST-URANS

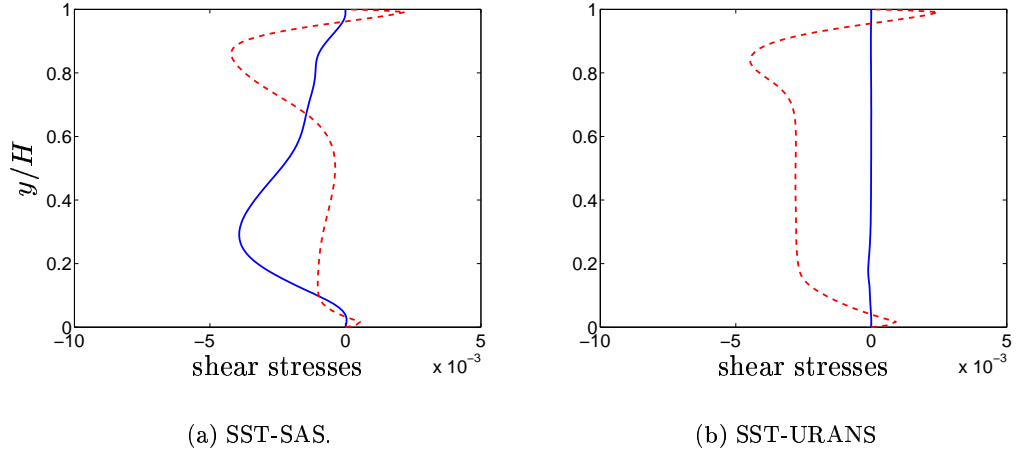


Figure 22: Shear stresses. — : resolved; - - - : modelled.  $x = H$ .

model, especially in the stagnant region in the middle of the room. Here the turbulent transport of momentum due to resolved fluctuations is larger than that due to modelled fluctuations. The resolved fluctuations predicted with the SST-URANS model are close to zero everywhere.

The SAS term is expressed as the ratio of the von Kármán length scale,  $L_{vk,3D}$ , and the usual RANS turbulent length scale  $c_\mu^{-1/4} k^{1/2} / \omega$ . The von Kármán length scale is evaluated using data from a DNS simulation and from a hybrid LES-RANS simulation. It is found that when using the DNS data the von Kármán length scale expressed in instantaneous velocity gradients closely follows the smallest grid spacing, i.e. the wall-normal spacing,  $\Delta y$ . When using the hybrid LES-RANS data the von Kármán length scale in the wall region (i.e. the URANS region) is slightly larger than  $\Delta y$  because of rather larger turbulent viscosities which makes the smallest, resolved scales larger.

The concept of using the von Kármán turbulent length scale for detecting unsteadiness is very interesting. This idea should be pursued further and could be used in connection with other models. In the SST-SAS model the von Kármán length scale is used to trigger an additional source term. As an alternative it could probably also be used for changing the value of a coefficient in a transport turbulence model.

## References

- Billson, M., 2004. Computational techniques for turbulence generated noise. Ph.D. thesis, Dept. of Thermo and Fluid Dynamics, Chalmers University of Technology, Göteborg, Sweden.
- Billson, M., Eriksson, L.-E., Davidson, L., 2003. Jet noise prediction using stochastic turbulence modeling. AIAA paper 2003-3282, 9th AIAA/CEAS Aeroacoustics Conference.
- Davidson, L., Billson, M., 2006. Hybrid LES/RANS using synthesized turbulence for forcing at the interface (to appear). *International Journal of Heat and Fluid Flow*.
- Davidson, L., Farhanieh, B., 1995. CALC-BFC: A finite-volume code employing collocated variable arrangement and cartesian velocity components for computation of fluid flow and heat transfer in complex three-dimensional geometries. Rept. 95/11, Dept. of Thermo and Fluid Dynamics, Chalmers University of Technology, Gothenburg.
- Davidson, L., Peng, S.-H., 2003. Hybrid LES-RANS: A one-equation SGS model combined with a  $k - \omega$  model for predicting recirculating flows. *International Journal for Numerical Methods in Fluids* 43, 1003–1018.
- Emvin, P., 1997. The full multigrid method applied to turbulent flow in ventilated enclosures using structured and unstructured grids. Ph.D. thesis, Dept. of Thermo and Fluid Dynamics, Chalmers University of Technology, Göteborg.
- Menter, F., 1994. Two-equation eddy-viscosity turbulence models for engineering applications. *AIAA Journal* 32, 1598–1605.
- Menter, F., Egorov, Y., 2004. Revisiting the turbulent length scale equation. In: *IUTAM Symposium: One Hundred Years of Boundary Layer Research*. Göttingen.
- Menter, F., Egorov, Y., 2005. A scale-adaptive simulation model using two-equation models. AIAA paper 2005-1095, Reno, NV.
- Menter, F., Kuntz, M., Bender, R., 2003. A scale-adaptive simulation model for turbulent flow prediction. AIAA paper 2003-0767, Reno, NV.
- Rotta, J., 1972. *Turbulente Strömungen*. Teubner Verlag, Stuttgart.



